ACS Infectious Diseases

pubs.acs.org/journal/aidcbc

Article

Synthesis and Characterization of DOTAM-Based Sideromycins for Bacterial Imaging and Antimicrobial Therapy

Carsten Peukert, Katharina Rox, Bianka Karge, Sven-Kevin Hotop, and Mark Brönstrup*

Cite This: *ACS Infect. Dis.* 2023, 9, 330−341

Read Online

ACCESS | Metrics & More | Article Recommendations | Supporting Information

ABSTRACT: The rise of antimicrobial resistance, especially in Gram-negative bacteria, calls for novel diagnostics and antibiotics. To efficiently penetrate their double-layered cell membrane, we conjugated the potent antibiotics daptomycin, vancomycin, and sorangicin A to catechol siderophores, which are actively internalized by the bacterial iron uptake machinery. LC−MS/MS uptake measurements of sorangicin derivatives verified that the conjugation led to a 100- to 525-fold enhanced uptake into bacteria compared to the free drug. However, the transfer to the cytosol was insufficient, which explains their lack of antibiotic efficacy. Potent antimicrobial effects were observed for the daptomycin conjugate **7** (∼1 μM) against multidrug-resistant *Acinetobacter baumannii*. A cyanin-7 label aside the daptomycin warhead furnished the theranostic **13** that retained its antibiotic activity and was also able to label ESKAPE bacteria, as demonstrated by microscopy and fluorescence assays. **13** and the cyanin-7 imaging conjugate **14** were stable in human plasma and had low plasma protein binding and cytotoxicity.

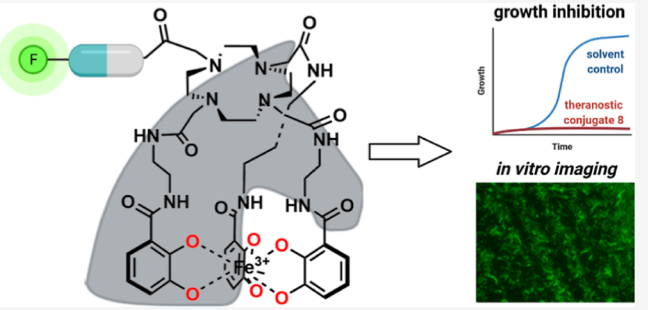

KEYWORDS: *theranostic, siderophores, Trojan horse, drug delivery, antibiotic conjugates, diagnostics*

The escalating antibiotic resistance has become a major global health challenge that will probably prevail in the decades to come. The consequences of antimicrobial resistance caused 1.27 million deaths in 2019 alone, and there is a severe economic damage in addition.[1] An innovation gap over the past 3−4 decades, which followed the so-called golden era of antibiotics, laid the foundation for this scenario.[2] In 2017, the World Health Organization published a priority list of antibiotic-resistant bacteria, which included multidrug-resistant (MDR) *Acinetobacter baumannii*, *Pseudomonas aeruginosa*, and Enterobacteriaceae as strains of critical concern.[3] For these Gram-negative species, the need for novel antibiotics, drug delivery systems, and innovative bacterial diagnostics is regarded as particularly high.[2,4] Scientists have exploited bacterial transporters and their substrates to increase the accumulation of various payloads for bacterial imaging or antibacterial treatment into the pathogens.[5] Among those, iron transporters play a role in the competition for the metal between a host organism and the invading pathogenic bacteria and for the outcome of an infection.[6,7] The insolubility of Fe(III) required prokaryotes to evolve sequestration processes that involve the active transport of the so-called siderophores, iron chelators of medium molecular weight. Gram-negative bacteria recognize ferric siderophore complexes by chelator-specific outer membrane receptors (OMRs). Binding to the OMR initiates the energy-dependent translocation of the complex into the periplasm and often to the inner membrane.[6] Many bacteria commit "iron thievery" by hijacking the siderophores from other bacterial species (xenosiderophores); also, synthetic siderophore mimics are transported by OMRs.[8,9] Some microbes secrete covalent conjugates of antibiotic molecules and siderophores, called sideromycins, that confer advantages to the producer strain. Numerous research groups leveraged the potential of siderophores as molecular "Trojan Horses" to smuggle diagnostic and therapeutic payloads into the bacterial cell (Figure 1A), thereby overcoming the reduced permeability into Gram-negative prokaryotes. Most conjugates employed well-characterized antibiotics (e.g., β-lactams) and intended to enhance their activity by an improved, bacteria-specific active uptake.[10] Accordingly, siderophore conjugation may repurpose Gram-positive-only antibiotics, which show limited bacterial accumulation due to their high molecular weight, overall charge, or lipophilicity, and unfold their potential to combat Gram-negative infections. The potent siderophore conjugates of the bulky lipopeptides daptomycin and teicoplanin, exhibiting nanomolar minimal inhibitory concentration (MIC) values in MDR *A. baumannii*, impressively confirmed the feasibility of

Received: October 17, 2022
Published: January 31, 2023

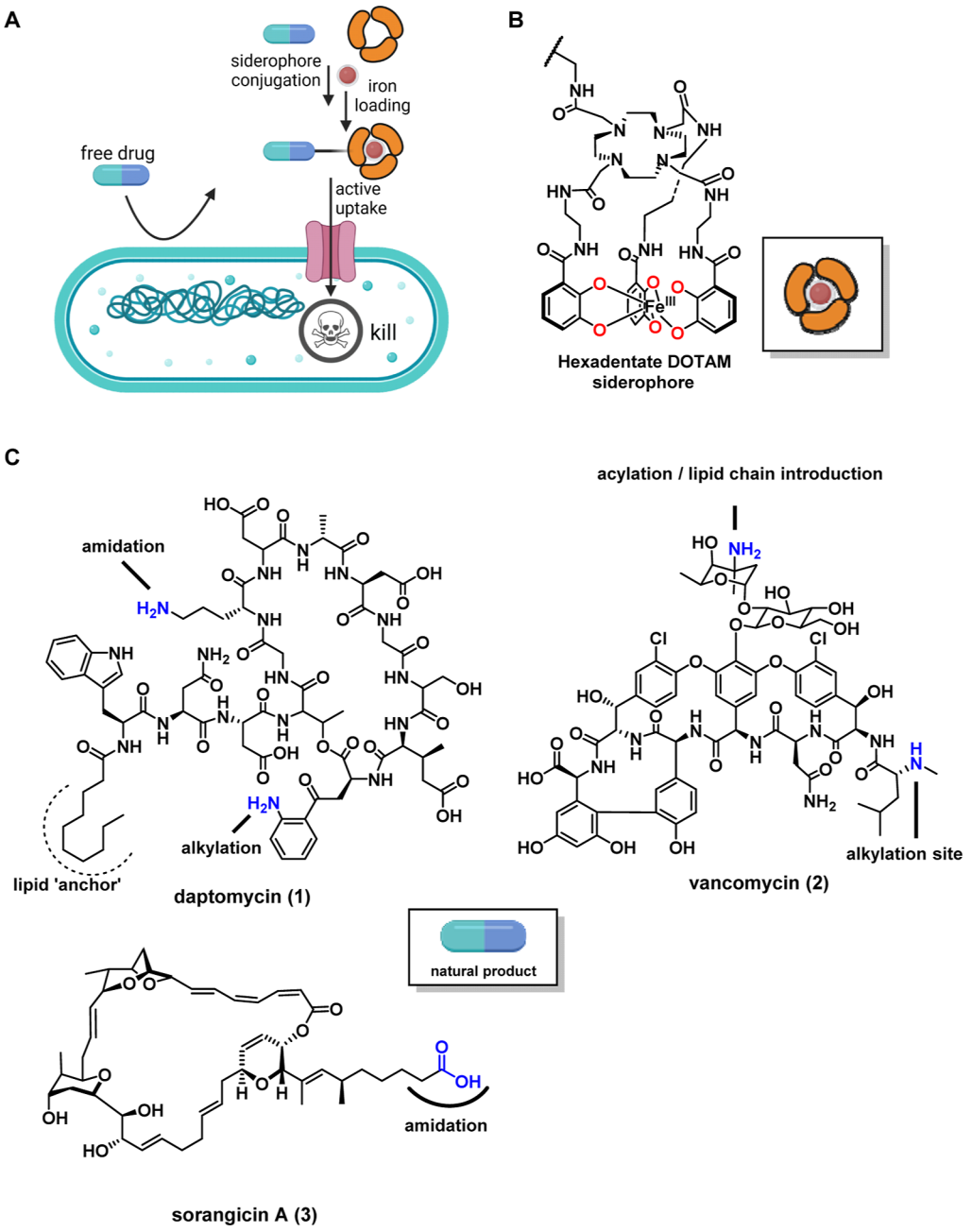

Figure 1. Conjugation of siderophores to natural products with exclusive activity in Gram-positive bacteria. (A) Schematic depiction of enhanced bacterial accumulation and antibiotic activity through siderophore conjugation. (B) Structure of the synthetic hexadentate DOTAM siderophore. (C) The lipopeptide daptomycin, the glycopeptide vancomycin, and the macrolide sorangicin A are potent antibiotics against Gram-positive bacteria but inactive against Gram-negative pathogens. Possible modification sites for a conjugation to "Trojan Horses" are highlighted in blue.[16−18]

the above strategy.[11−14] In some cases, the iron-binding catechol moieties of the siderophore were masked as a prodrug by acetylation to avoid in vivo deactivation of the iron chelator by catechol-*O*-methyltransferases.[15] Depending on the assay and/or the compound, the prodrug form is sometimes—but not always—superior to the free catechol; therefore, both versions are often prepared. Siderophore conjugates are mostly used in their apo-form, and the metal is bound in situ, capturing residual iron from the culture medium.

Recently, we developed the DOTAM (1,4,7,10-tetraazacyclododecane-1,4,7,10-tetraacetic acid amide) core as an effective carrier for bacteria-specific imaging as well as for bacterial killing (Figure 1B).[19−22] While a conjugate enrichment into pathogenic microbes via active transporters for either therapeutic or diagnostic purposes has been leveraged widely, a combination of both functionalities to a theranostic that can treat and monitor an infection herd simultaneously has remained largely unexplored, apart from few, recently published examples.[23−25] Therefore, we aimed to equip a potent antimicrobial with a fluorescent imaging modality to afford such a theranostic molecule. In this study, we describe the synthesis, antibiotic potential, and accumulation of high molecular weight DOTAM natural product conjugates against Gram-negative pathogens.

https://doi.org/10.1021/acsinfecdis.2c00523
ACS Infect. Dis. 2023, 9, 330−341

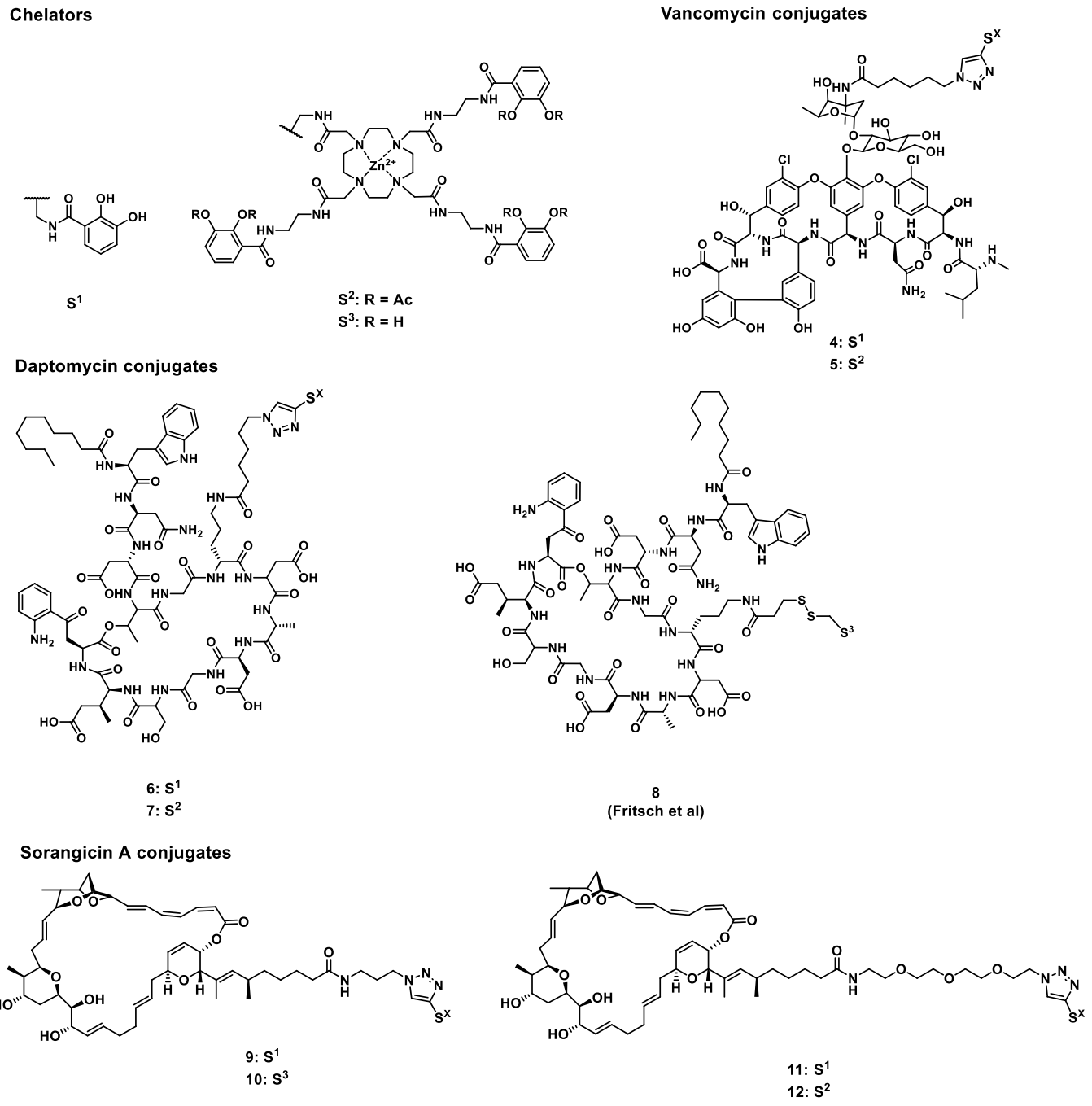

Figure 2. Structures of synthetic vancomycin, daptomycin, and sorangicin A conjugates.

RESULTS AND DISCUSSION

We selected the lipopeptide antibiotic daptomycin (**1**, 1620.7 Da), the glycopeptide vancomycin (**2**, 1447.4 Da), and the macrolide sorangicin A (**3**, 806.5 Da), which are all very potent antibiotics with submicromolar MIC values but are solely effective in Gram-positive bacteria (Figure 1C). Daptomycin interacts with the lipid phosphatidylglycerol in a calcium-dependent manner, while its lipid anchor allows the insertion into the Gram-positive cell membrane, thereby disturbing intracellular homeostasis.[26−28] Vancomycin exerts its effect by binding to the C-terminal D-Ala-D-Ala motif of the Gram-positive cell wall precursors, leading to an inhibition of the peptidoglycan crosslinking by the transpeptidase.[29,30] The myxobacterial natural product sorangicin inhibits the DNA-dependent RNA polymerase (RNAP) in the cytosol by blocking the RNA transcript elongation at a length of two to three nucleotides.[31] Although the compound occupies a similar position as the well-studied rifamycin, its cellular mode of action is different.[18,31−33] We anticipated the risk that the attachment of the bulky DOTAM chelator to any of the effectors could impact their target-binding ability due to its steric demand. For this reason, either a full DOTAM siderophore or a monocatechol was attached to the peripheral moieties of all effectors (Figure 2). The alkyne-tagged DOTAM siderophore **18** was synthetized as previously described, and the alkyne-tagged monocatechol **16** was afforded over two steps from **15** (Figure S1).[19] Previous structure−activity relationship studies demonstrated that

https://doi.org/10.1021/acsinfecdis.2c00523
ACS Infect. Dis. 2023, 9, 330−341

Table 1. Antimicrobial Activity of Daptomycin 1, Vancomycin 2, and Their Conjugates 4−8[a]

strain	4	5	6	7	8	dapto (1)	vanco (2)	cef
E. coli DSM1116	>20	>20	>20	>20	>20	>20	>20	0.1
S. aureus DSM11822	**21.8**	**6.1**	**14.0**	**5.5**	**11.8**	**0.3**	**0.5**	>8.5
K. pneumoniae DSM11678	>20	>20	>20	>20	>20	>20	>20	0.2
A. baumannii DSM30007	>20	>20	**12.3**	**1.6**	**1.5**	>20	>20	0.1
A. baumannii DSM30008	>20	>20	>20	**1.3**	**2.5**	>20	>20	0.1
P. aeruginosa DSM117	>20	>20	>20	>20	>20	>20	>20	0.2
E. faecium DSM20477	>20	>20	>20	>20	>20	**0.9**	**0.3**	>8.5

[a]Values in [μM], n = 3, in IDCAM, 110 μg/mL $CaCl_2$ addition[26] for the daptomycins **1** and **6**−**8**. Daptomycin (dapto), vancomycin (vanco), and cefiderocol (cef) were used as standard antibiotics.[36]

Table 2. Antimicrobial Activity of Sorangicin A (3) and Its Siderophore Conjugates 9−12[a]

strain	9	10	11	12	sorA (3)	cef
E. coli DSM1116	>20	>20	>20	>20	**3.13**	**0.1**
S. aureus RKI 11-02670	**18**	2			0.15	
S. aureus DSM11822	**37.5**	**0.78**	**6.7**	**3.5**	**0.2**	>8.5
K. pneumoniae DSM11678			>20	>20	>20	**0.2**
A. baumanniiDSM30007			>20	>20	>20	0.2
A. baumannii DSM30008			>20	>20	>20	0.1
P. aeruginosa DSM117	>20	>20	>20	>20	>20	**0.2**
E. faeciumDSM20477			**6.7**	**3.5**	**0.15**	>8.5

[a]Values in [μM], n = 3, in IDCAM. Sorangicin A (sorA) and cefiderocol (cef) were used as standard antibiotics.

amide coupling of the ornithine side chain in daptomycin preserved the antibacterial activity in Gram-positive bacteria.[27] Similarly, a vancomycin modification at the peripheral disaccharide entity was found to be well tolerated.[34,35] Therefore, **1** and **2** were modified at their primary amine moieties with NHS- or PFP-activated 6-azido hexanoic acid in yields of 46 and 25%, respectively, and then coupled to siderophores through copper-catalyzed azide alkyne cycloadditions (CuAACs).

The vancomycin−catechol conjugate **4** and the vancomycin−DOTAM conjugate **5** were synthetized over four to six steps with 5−20% overall yield. The daptomycin−catechol conjugate **6** and the daptomycin−DOTAM conjugate **7** were synthetized over four to six steps with 23 and 19% overall yield, respectively. Also, the daptomycin−DOTAM conjugate **8** with a cleavable disulfide linker could be afforded over seven steps with 17% yield, as reported recently.[22] In the case of sorangicin A, the molecule's acid moiety was modified either with an azido propan-1-amine or with an azido-PEG_3-amine linker, which was then conjugated through CuAAC to **16** or **18**. The alkyl-linked monocatechol **9** and the DOTAM **10** could be afforded over two steps each with 28 and 43% overall yield, respectively. Sorangicin A conjugates with a longer NH_2-PEG_3-N_3 linker could be synthetized via a similar route with 79% (catechol **11**) and 84% (DOTAM **12**) yield over two steps.

We next determined the antimicrobial activities of the conjugates that reflect their ability to translocate into bacteria but also to inhibit their targets. The MICs of all conjugates were evaluated in iron-depleted, cation-adjusted medium (IDCAM). Siderophore conjugation did not enhance the activity of vancomycin conjugates **4** and **5**. In contrast, the daptomycin−DOTAM conjugates **7** and **8** exhibited potent, single-digit micromolar MICs in two MDR *A. baumannii* strains in $CaCl_2$ supplemented media (Table 1). The cleavable disulfide linker in **8** did not lead to a significant improvement in activity compared to the non-cleavable linker of **7**, in accordance with previous reports.[12] Possibly, the ferric complex formation required for uptake via a siderophore transporter in the case of the daptomycin monocatechol **6** only leads to a moderate increase in potency. The MICs against *S. aureus* were generally higher for the conjugates than for the unmodified drugs **1** or **2**.[11] Overall, the increased potency of three conjugates against *A. baumannii* demonstrates the ability of the DOTAM siderophore to improve translocation into this species. However, although a universal OMR binding motif in the form of catechols was presented, the activity could not be obtained against all Gram-negative bacteria.

The covalent chelator conjugation to the RNAP inhibitor sorangicin did not enhance the activity in Gram-negative bacteria; the moderate activity of **3** against *Escherichia coli* was even lowered by conjugation (Table 2). In Gram-positive strains, **9**, **10**, **11**, and **12** retained the activity, although the potency was lowered in comparison with unmodified sorangicin A. In general, the modification of the carboxylic acid of **3** with a linker by amide formation consistently reduced the activity.

The lack of a potency boost upon chelator conjugation to sorangicin could be attributed to three major reasons: (i) the chemical modification impeded target engagement, (ii) the uptake into bacteria was inefficient, or (iii) the transport across the outer membrane occurred, but the conjugates could not reach the cellular compartment of their target in sufficient quantity. To investigate the latter two options, an uptake assay based on a combination of cellular fractionation with liquid chromatography coupled to tandem mass spectrometry (LC−MS/MS) was conducted in enterobactin-deficient *E. coli* Δ*entA* in iron-free media, with or without 10 μM $FeCl_3$ supplementation.[37] The bacteria were incubated with **3**, **9**, or **10** (50 μg/mL) for 10 min and perforated by an osmotic shock to release the periplasmic fraction by centrifugation. A sonication−centrifugation procedure yielded separate membrane and cytosolic fractions. Mass spectrometric quantitation revealed a strong enrichment of the sorangicin A conjugates in the membrane and periplasmic fractions, with minor

https://doi.org/10.1021/acsinfecdis.2c00523
ACS Infect. Dis. 2023, 9, 330−341

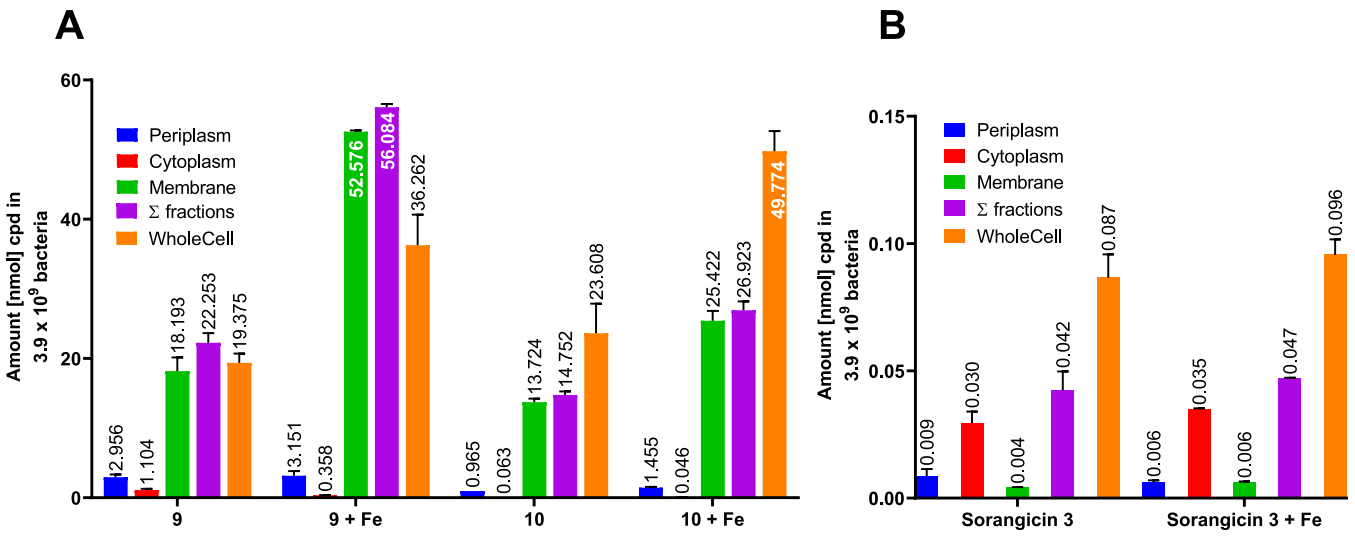

Figure 3. Intracellular accumulation of **3**, **9**, and **10** in *E. coli*. Following the incubation of *E. coli* Δ*entA* with the test compounds (±10 μM $FeCl_3$), the bacterial compartments were fractionated, and their amount was quantified by LC−MS/MS, $n = 2$.

accumulation in the cytoplasmic fractions. The addition of ferric iron increased the accumulation of conjugates **9** and **10** inside of the bacteria but expectedly had no effect on the accumulation of the unmodified natural product due to the missing siderophore entity (Figure 3).

Generally, the conjugation to a chelator increased compound lipophilicity and manifested in higher membrane accumulation. The comparison of the cytoplasmic amounts of the conjugates with those of the unmodified natural product **3** showed an increased accumulation of **9** (11- to 36-fold) and **10** (~2-fold) at their target site in the cytosol. In the periplasm, **9** and **10** displayed a 100- to 525-fold enrichment compared to free sorangicin A. The data demonstrate that already the addition of a monocatechol and also of a DOTAM chelator boosted the accumulation of the natural product significantly. This underlines the general ability of DOTAM to act as a molecular "Trojan Horse", efficiently transporting cargo into bacterial cells. However, the relative ratio of compound amounts in the cytoplasm compared to the periplasm was lowered upon conjugation, whereas **3** had a cytoplasm/periplasm ratio of 3−5:1 but only 0.1−0.4:1 for **9**, and 0.03−0.07:1 for **10**. Because the periplasm has a much smaller volume than the cytoplasm, the differences in concentrations c were even more pronounced: The ratio c_{cyto}/c_{peri} was 27−45:1 for **3** but only 0.8−3:1 for **9** and 0.2−0.5:1 for **10**. We conclude that the DOTAM-based siderophore mimics functioned well with respect to the transport across the outer membrane, but their efficiency with respect to the cytoplasmic delivery of sorangicin was insufficient.

From the first panel of compounds, we selected the daptomycin DOTAM conjugate **7** as a blueprint for the construction of a theranostic. In particular, we envisioned a combination of the DOTAM-conjugated daptomycin warhead with a fluorescent cyanin-7 infrared imaging label to visualize and treat *A. baumannii* infections simultaneously. We assumed that the combination of three bulky components, that is, a bulky DOTAM carrier, a fluorophore, and the big polypeptide daptomycin, in one conjugate might significantly reduce the antibiotic efficacy due to steric hindrance. Therefore, a conjugate with a longer spacer between the siderophore and the crosslinker with the attached fluorophore and antibiotic was designed to permit for an unperturbed target binding compared to **7** (Figure 4). The synthesis commenced with the amide coupling with the mono-Boc-protected 1,6-diaminohexane to N^{α}-Fmoc-N^{δ}-azido-D-ornithine, whose Fmoc group was subsequently cleaved to afford amine **24**. Reaction of the primary amine with the active succinimidyl ester of cyanin-7 and strain-promoted azide−alkyne cycloaddition (SPAAC) with DBCO-daptomycin **25** yielded the difunctionalized fragment **27a**. Boc group cleavage and modification with *N*-hydroxy succinamide-activated DBCO afforded amide **27b** in 67% yield over two steps. Another SPAAC with the previously published azido DOTAM **28** furnished the full theranostic conjugate **13** in 32% yield over seven synthetic steps for the longest linear sequence.[20] CuAAC of commercial cyanin-7 azide to alkyne **19** afforded imaging conjugate **14** in 80% yield.

We tested whether the theranostic **13** and the imaging probe **14** were able to label iron-starved, MDR bacteria (Figure 5). A quantitative readout displayed a rather homogeneous fluorescence signal for **14** in all ESKAPE pathogens (*E. coli*, *S. aureus*, *K. pneumoniae*, *A. baumannii*, *P. aeruginosa*, and *Enterococcus faecium*). The signal from **13** with its much higher molecular weight was 5.5- to 15.3-fold lower than that for **14**. Surprisingly, the theranostic had a 2- to 3-fold higher fluorescence signal for its target species *A. baumannii* than for the other bacteria (p-value < 0.0001). The labeling of *A. baumannii* by **13** and **14** was also confirmed by fluorescence microscopy experiments. For the imaging probe **14** that gave higher intensities in the plate assay, microscopy pictures were obtained for the whole ESKAPE panel (Figure S5). Varying staining efficiencies were observed, and in many cases, subpopulations within a given strain were labeled differentially. This heterogeneity on the single-cell level might reflect varying conjugate uptake or growth phases.

Next, we aimed to evaluate the antimicrobial activity of **13** and **14** under iron-depleted conditions against *A. baumannii* (DSM30007). Conjugates were evaluated twofold: (i) either in an 18 h growth kinetic with shaking or (ii) in a single-endpoint measurement after 18 h without shaking (Figure 6). Expectedly, **14** did not affect the microbial growth, while the growth control and the control antibiotics had activity in the expected ranges (Figure S6). Despite the moderate growth reduction

https://doi.org/10.1021/acsinfecdis.2c00523
ACS Infect. Dis. 2023, 9, 330−341

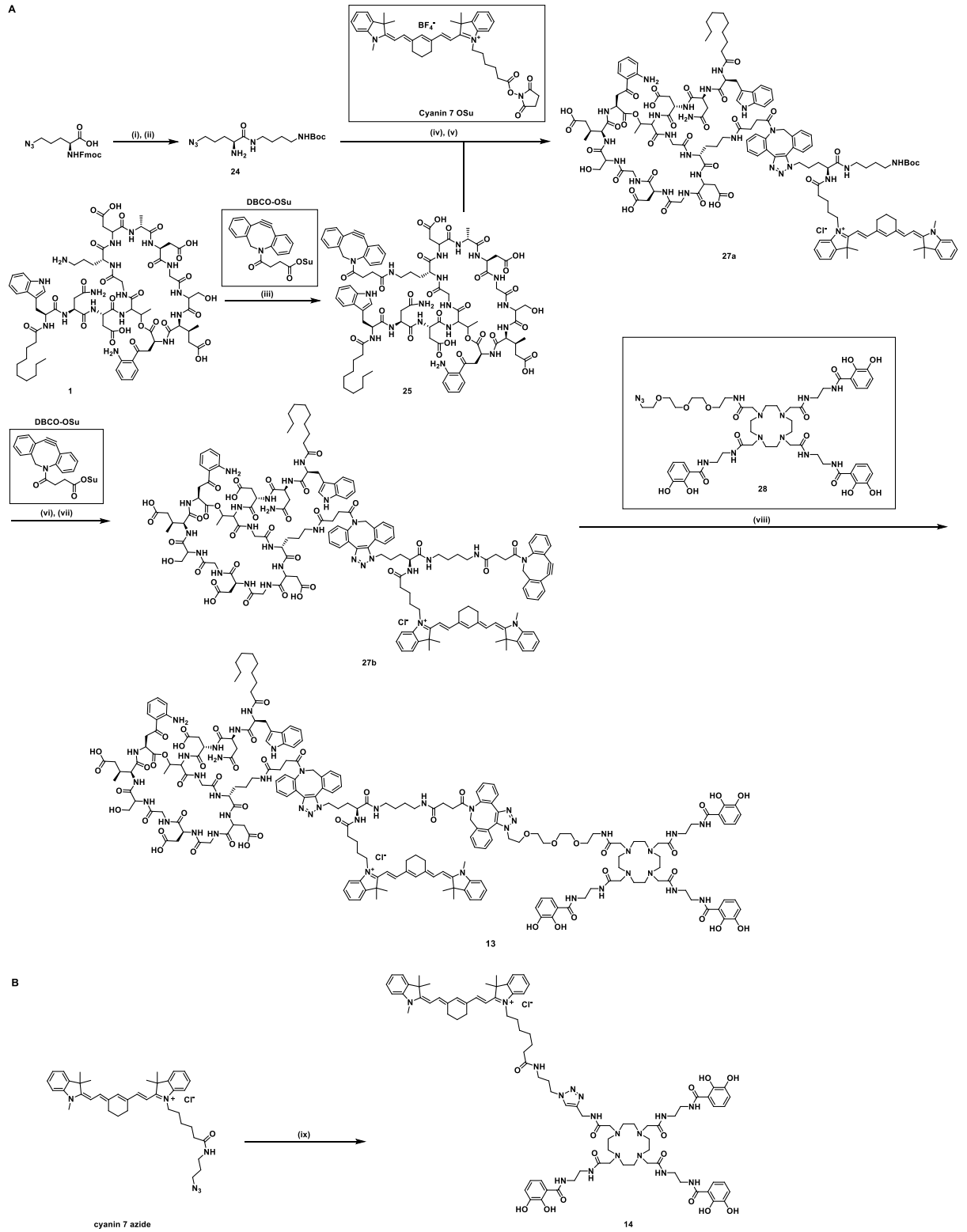

Figure 4. Synthesis of the DOTAM-based theranostic **13** and the imaging conjugate **14**. (A) Theranostic **13**: (i) *N*-boc-1,6 diaminohexane, HATU, DIPEA, DCM, DMF, 22 °C; (ii) 20% diethylamine in acetonitrile (ACN), 22 °C, 2 h, 87% over two steps; (iii) **DBCO-OSu**, *N*,*N*-diisopropylethylamine (DIPEA), dimethyl sulfoxide (DMSO), 23 °C, overnight, crude quant.; (iv) **cyanin 7-OSu**, DCM, DIPEA, 23 °C, 2 h; (v) MeOH, overnight, 23 °C, quant. over two steps; (vi) 20% TFA, DCM, 23 °C; (vii) **DBCO-OSu**, DCM, DMF, DIPEA, 23 °C, 67% over two steps; and (viii) MeOH, 23 °C, overnight, 85%, and (B) imaging conjugate **14**: (ix) **19**, $Zn(OAc)_2$, $CuSO_4$, sodium ascorbate, DMF/Milli-Q H_2O, (1:1), TBTA, 23−30 °C, 2 h, 80%.

observed for free daptomycin at the highest concentration, no concentration could inhibit the growth completely, confirmed by the single-point measurement (Figure 6). In contrast, the theranostic **13** reduced the bacterial growth in the kinetic as well as in the endpoint experiment at a concentration of 8−16 μM. This corresponds to a ca. 8-fold increase in MIC

https://doi.org/10.1021/acsinfecdis.2c00523
ACS Infect. Dis. 2023, 9, 330−341

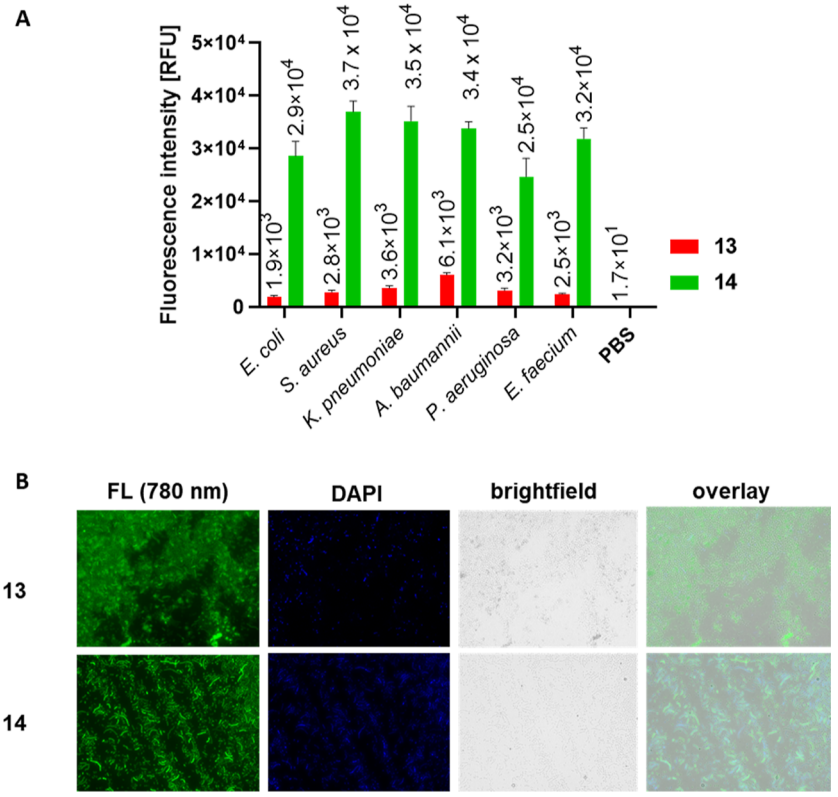

Figure 5. Labeling of bacterial pathogens with fluorescent DOTAM conjugates **13** and **14**. (A) Fluorescence intensity [RFU] of ESKAPE pathogens after incubation with **13** and **14** (10 μM) in IDCAM, with λ_{Ex} = 735 nm and λ_{Em} = 780 nm. Error bars correspond to ±standard error of mean (SEM), n = 3. (B) Fluorescence microscopy images (FL 780 nm) of *A. baumannii* (DSM30007) after incubation with **13** and **14** (10 μM) in IDCAM. Also, DAPI fluorescence, the brightfield image, and the overlay of all the three images are shown. Representative examples of two experiments are given. Microscopic pictures for **14** in the full ESKAPE panel are given in the Supporting Information.

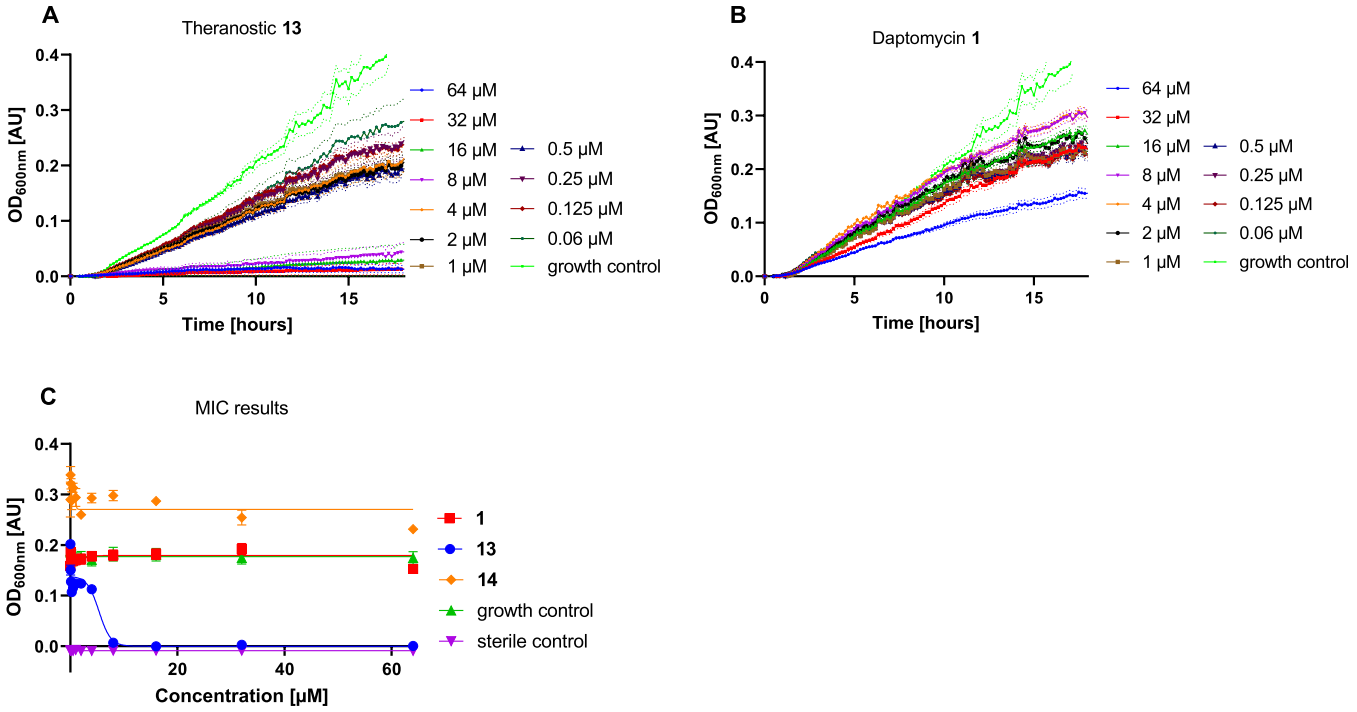

Figure 6. Antimicrobial activity of **13**, **14**, and **1** against *A. baumannii* (DSM30007). Growth kinetics (OD_{600nm}) of **13** (A) and **1** (B) in iron-depleted, cation-adjusted medium (IDCAM, with 110 μg/mL $CaCl_2$) over 18 h at 37 °C. Dotted lines correspond to ±SEM, n = 3. Minimal inhibitory concentration assay (C) of **13** and **1** in IDCAM (IDCAM, with 110 μg/mL $CaCl_2$), without shaking at 37 °C, error bars correspond to ±SEM, n = 3. Curves for the positive control ciprofloxacin are shown in Figure S6.

https://doi.org/10.1021/acsinfecdis.2c00523
ACS Infect. Dis. 2023, 9, 330−341

Table 3. Plasma Stability, Plasma Protein Binding, and Cytotoxicity in Four Eukaryotic Cells of Selected Conjugates

	1	13	14	27a	27b
PPB human [%]	98.8 ± 0.1	49.7 ± 1.2	94.5 ± 0.5	91.6 ± 3.7	82.6 ± 14.2
half-life in mouse plasma [min]	>240	35.1	>240	>240	>240
half-life in human plasma [min]	>240	>240	>240	>240	>240
	cytotoxicity [μM]				
	1	13	14	staurosporine	auranofin
L929 cells	64	64	64	<0.064	0.1
A549 cells	>64	64	64	0.05	0.1
KB-3-1 cells	>64	>64	64	0.004	0.1
MCF-7 cells	>64	>64	>64	0.002	0.05

compared to **7**, the conjugate without the imaging label. Thus, the attachment of the cyanin-7 dye had a negative effect on either target binding or accumulation. Upon testing of **13** in iron-rich MHB, no antimicrobial activity was observed, indicating a central role of the ferric siderophore uptake machinery in bacterial enrichment and antibacterial activity (Figure S6C). Daptomycin **1** expectedly remained inactive under these iron-rich testing conditions.

The cytotoxicity of the theranostic **13** and the imaging conjugates **14** and **1** was tested in four eukaryotic cell lines: L929, A549, KB-3-1, and MCF-7. All conjugates as well as **1** were non-cytotoxic up to concentrations ≥ 64 μM (Table 3). Moreover, we assessed the stability of **13**, **14**, the theranostic intermediates **27a**/**27b**, as well as daptomycin **1** in mouse and human plasma. For this purpose, compounds were incubated in plasma at 37 °C for up to 240 min. At the time points t = 0, 15, 30, 60, 120, and 240 min, the samples were taken, extracted using ACN, dried under nitrogen to avoid degradation during HPLC−MS/MS measurements, dissolved in DMSO, and measured using targeted MS/MS with multiple reaction monitoring (MRM), with at least two MS/MS pairs for each compound (Table S3). None of the conjugates or theranostic fragments showed liabilities with respect to plasma stability, as all compounds were stable for more than 240 min (Table 3). The theranostic **13** was fully stable in human plasma but exhibited a limited half-life of 35 min in mouse plasma. We also determined the human plasma protein binding, as only the free fraction may exert an effect as a theranostic. Whereas more than 98% of **1** was bound to plasma proteins, **14** showed a lower binding of less than 95%. The theranostic **13** showed an even lower human plasma protein binding of only 49.7%, and the intermediates **27a** and **27b** exhibited a plasma protein binding of 91.6 and 82.6%, respectively. Taken together, **13** and **14** exhibited good antibiotic and labeling activities, respectively, and low cytotoxicity qualifies them for future in vivo testing. The instability of **13** in mouse plasma would either require further medicinal chemistry efforts to improve the stability before evaluating the efficacy in a mouse infection model or could possibly be bypassed through the usage of humanized mice.

CONCLUSIONS

We explored whether the antibiotic potency of three well-established classes of natural products against Gram-negative bacteria could be enhanced by conjugation to a DOTAM triscatecholate or a monocatechol unit. Most conjugates had reduced activity in Gram-positive strains, and also the Gram-negative activity was enhanced in only few cases. For sorangicin conjugates, we demonstrated by quantitative uptake measurements that the siderophore improved the translocation across the outer membrane significantly, but the passage across the inner membrane to the cytosol remained insufficient. The finding is in line with a general observation for most covalent siderophore conjugates, that is, that antibiotic activity is by and large poor when cytosolic targets are addressed. This implies that for siderophore conjugates acting in the cytosol, the passage across the inner membrane needs to be considered - a mechanism that is mostly not understood and neglected. Alternatively, such conjugates may require or strongly benefit from an intracellular release mechanism for the antibiotic from the carrier to ensure activity.

The daptomycin DOTAM conjugate **7** had potent activity against antibiotic-resistant *A. baumannii* and thus was equipped with a cyanin-7 fluorophore to yield the theranostic **13**. This large conjugate retained potency and could detect, alike imaging compound **14**, Gram-negative and Gram-positive ESKAPE bacteria in the culture. Both conjugates showed no cytotoxicity and exhibited sufficient stability in human plasma and thus are interesting candidates for in vivo experiments.

In sum, we expanded the application of the DOTAM siderophore as a versatile and functional carrier even for bulky payloads, such das daptomycin or sorangicin A, for therapeutic and diagnostic purposes.[19] Future attempts could, in accordance with previous studies, incorporate a radioactive label such as copper-64 directly at the cycle instead of the bulky cyanin-7, which in turn would facilitate the synthesis and reduce structural alterations.[16]

METHODS

Chemical Methods. Unless otherwise mentioned, reagents were purchased and used without further purification. All employed solvents for workups and purifications were p.a. or HPLC purity grade. The DOTAM siderophores were synthetized as described in Ferreira et al.[19,40] and Peukert, Langer et al.[20] The synthesis procedures of other intermediates and conjugates are described in the Supporting Information. All isolated compounds were characterized by ^{1}H NMR (all compounds), ^{13}C NMR (molecular weight < 1300 g/mol and selected compounds) spectra, and ESI-HRMS (all compounds). The yields are calculated based on substance purity ≥ 95% as confirmed by NMR and MS.

MIC Tests in Iron-Depleted, Cation-Adjusted Medium. The MIC was determined in IDCAM, as previously described by Pinkert, Lai et al.[14,38] Used strains are shown in the Supporting Information in Table S1.

Quantification of Sorangicin and Derivatives in the Subcellular Compartments of *E. coli* ΔentA. The compounds were quantified using our previously described protocol for strain cultivation, incubation, and cellular fractionation.[37] In brief, a culture of *E. coli* ΔentA (CGSC3

https://doi.org/10.1021/acsinfecdis.2c00523
ACS Infect. Dis. 2023, 9, 330−341

11768) was grown in LB media overnight. On the following day, the culture was started in LB media at OD_{600} = 0.2 until it reached OD_{600} = 0.8. Cells were washed twice with LMR media without $FeCl_3$ and centrifuged at 4500*g*.[39] Afterward, the cells were adjusted to OD_{600} = 1.0 in LMR media (∓10 μM $FeCl_3$) and incubated with 50 μg/mL respective compound for 10 min. Thereafter, the cells were handled according to the protocol used by Prochnow et al.[37]

LC−MS/MS measurements were carried out on a UHPLC (Agilent 1290, Agilent Technologies, Santa Clara, CA, USA) coupled to a triple quadrupole mass spectrometer (QTrap 6500, AB Sciex GmbH, Darmstadt, Germany). The LC separations were conducted with a linear gradient of solvent A (H_2O + 0.1% HCOOH) and solvent B (can + 0.1% HCOOH) from 1% B to 99% B within 8.5 min at a flowrate of 0.7 mL/min on a YMC-Pack TMS 100 mm × 2.1 mm/S3 μm/12 nm column (YMC Europe, Dinslaken, Germany) equipped with a guard column. A MRM method was used for compound detection in the positive and negative modes. The Q1/Q3 transition masses used for compound identification are given in Table S2. The reported data represent the average of two biological replicates performed on different days.

Cytotoxicity Testing. The effect of compounds on cell viability was probed with a WST-1 assay according to previously published procedures.[40,41] The following immortalized cell lines were used: Mouse fibroblast cell line L929 (DSM ACC 2), human cervix carcinoma cell line KB-3-1 (DSM ACC 158), human breast cancer cell line MCF-7 (DSM ACC 115), and human lung carcinoma cell line A549 (DSM ACC 107). Briefly, the subconfluent cells were washed with 1× PBS, trypsinized, and resuspended in Dulbecco's modified Eagle's medium that contained 5% FBS (L929, KB-31, A-549, and FS4-LTM) or the Roswell Park Memorial Institute medium that contained 5% FBS, 0.5% minimum essential medium non-essential amino acids, Gibco (MEM NEAA), 0.5% GlutaAC (Gibco), and insulin at 5 μg/mL (MCF-7). 25 μL of serial dilutions of the test compounds was added to 25 μL of a cell suspension (1500 cells for KB-31, A-549, and L929 and 3000 cells for MCF-7) in 384-well microtiter plates (final concentration range: 64−0 μM). Blank and solvent controls were incubated under identical conditions. The compounds (**1**, **13**, and **14**) were incubated for 24 h for the FS4-LTM cells and 5 days for the remaining cell lines. After the incubation period, 3 μL of WST-1 (ready-to-use solution from Roche) was added. The incubation time of the plates, which were briefly shaken at 37 °C, varied between the cell lines from 20 min for KB-3-1 up to 2 h for MCF-7 before measuring the absorption at 450 nm and reference at 600 nm with the Infinite 200 PRO Plate Reader (TECAN). The percentage of viable cells was calculated with respect to the solvent control (100% viability). EC_{50} values were determined with GraphPad Prism 8.

Fluorescence Assays. The bacterial strains were used and maintained at 37 °C in iron-depleted MHB (21 g/L Müller Hinton, pH 7.4, made iron-free by using CHELEX*). Before the assay, the strains were cultivated overnight in iron-free MHB at 37 °C and 180 rpm. The next morning, the overnight inoculum was diluted 1:25 in 10 mL of iron-free MHB in 100 mL Erlenmeyer flasks with chicane.

After ca. 4 h (OD_{600nm} range: 0.2−1.0), the inoculum was washed with 1× PBS (pH 7.4−3 × 25 mL/tube, 4500 rcf, 5 min, 4 °C), and then the pellet was diluted to an OD_{600nm} = 0.4 in iron-depleted MHB. The 10 mM compound stocks in DMSO (cell culture grade) were diluted in iron-depleted medium to yield a 20 μM intermediate solution, and 300 μL of each was distributed into 1.5 mL tubes.

The washed bacterial suspension was added to 20 μM compound in medium in a 1:1 dilution to yield OD_{600nm} = 0.2 and a compound concentration of 10 μM. For the solvent control, an equal amount of DMSO was diluted and added to the bacteria. Compound incubation was performed for 4 h at 30 °C and 200 rpm on a shaker. Then, bacteria were spun down and washed gently six times with 1 mL of 10% DMSO (v/v) in 1× PBS (pH 7.4−5 min, 4500 rcf, 4 °C, remove supernatant, add 1 mL, vortex 20 s). Low-binding tubes and tips were used and changed as often as possible to reduce artificial fluorescence readouts by residual dye sticking to the tubes.

The residual bacterial pellet was gently resuspended in 300 μL of fresh 10% paraformaldehyde solution (stored otherwise at −20 °C). This fixing buffer was supplemented with 3% glutaraldehyde; if the imaging facility was just S1 level, bacteria were incubated in this mixture overnight at 4 °C. In all cases, 3 μL of a ready-to-use solution of DAPI ROTIPHORESE solution was added and incubated for 30 min before pictures were taken. The imaging was performed in the fixation solution in ibidi 35 mm glass bottom dishes, or the sample was distributed into a black 96-well transparent bottom plate (150 μL/well) for quantitative analysis.

Plasma Stability. Each compound (**1**, **13**, **14**, **27a**, or **27b**) dissolved in DMSO was added to pre-warmed (37 °C) mouse (pH 7.4) or human plasma (pH 7.4) to yield a final concentration of 1 μM. In addition, procaine and procainamide (dissolved in DMSO) were added to mouse or human plasma (pH 7.4) to yield a final concentration of 1 μM. Procaine served as a positive control as it is unstable in mouse plasma. Procainamide served as a negative control as it is stable in mouse plasma. The samples were incubated for 0, 15, 30, 60, 90, 120, and 240 min at 37 °C. At each time point, 10 μL of the respective sample was extracted with 90 μL of ACN containing 12.5 ng/mL caffeine as an internal standard for 5 min at 2000 rpm on a MixMate vortex mixer (Eppendorf). ACN and caffeine were dispensed using a Mantis FORMULATRIX. The samples were centrifuged for 20 min at 2270 rcf at 4 °C, and the supernatants were transferred to 96-well Greiner V-bottom plates. Next, the samples were dried using N_2. Then, the samples were dissolved in 70 μL of DMSO per well. The samples were analyzed using HPLC−MS/MS analysis as described in the respective section. The peak areas of each compound and of the internal standard were analyzed using the MultiQuant 3.0 software (AB Sciex). The peak areas of the respective compound were normalized to the internal standard peak area and to the respective peak areas at time point 0 min: (C/D)/(A/B) with A: peak area of the compound at time point 0 min, B: peak area of the internal standard at time point 0 min, C: peak area of the compound at the respective time point, and D: peak area of the internal standard at the respective time point. Every experiment was repeated independently at least three times.

Plasma Protein Binding. Plasma protein binding was assessed using the rapid equilibrium device (RED) system from Thermo Fisher. Compounds **1**, **13**, **14**, **27a**, and **27b** were dissolved in DMSO. Naproxen served as a control as it shows high plasma protein binding. Compounds were diluted in human plasma (human donors, both genders, pooled) to a final concentration of 1 μM. Dialysis buffer and plasma

https://doi.org/10.1021/acsinfecdis.2c00523
ACS Infect. Dis. 2023, 9, 330−341

samples were added to the respective chambers according the manufacturer's protocol. The RED plate was sealed with a tape and incubated at 37 °C for 2 h at 800 rpm on an Eppendorf MixMate vortex mixer. Then, samples were withdrawn from the respective chambers. To 25 μL of each dialysis sample, 25 μL of plasma and to 25 μL of plasma sample, 25 μL of dialysis buffer were added. Then, 150 μL of ice-cold extraction solvent (MeCN/H_2O (90:10) containing 12.5 ng/mL caffeine as an internal standard) was added. The samples were incubated for 30 min on ice. Then, the samples were centrifuged at 4 °C at 2270 rcf for 10 min. Supernatants were transferred to Greiner V-bottom 96-well plates and sealed with a tape. Then, samples were subjected to HPLC−MS/MS analysis as described in the section "HPLC−MS/MS Analysis for Plasma Protein Binding and Plasma Stability Assays". The percentage of the bound compound was calculated as follows

$$f_{\text{bound}} = 100 - (c_{\text{buffer chamber}}/c_{\text{plasma chamber}}) \times 100$$

HPLC−MS/MS Analysis for Plasma Protein Binding and Plasma Stability Assays. LC/MS/MS measurements were carried out on a UHPLC (Agilent 1290 Infinity II, Agilent Technologies, Santa Clara, CA, USA) coupled to a triple quadrupole mass spectrometer (QTrap 6500plus or QTrap7500, AB Sciex GmbH, Darmstadt, Germany). The LC separations of **1**, **13**, **14**, **27a**, and **27b** were conducted with a linear gradient of solvent A (95% H_2O + 5% ACN + 5 mM NH_4COOCH_3 + 40 μL/L CH_3COOH) and solvent B (5% H_2O + 95% ACN + 5 mM NH_4COOCH_3 + 40 μL/L CH_3COOH) from 1% B to 99% B within 4.7 min. The LC separations for procaine, procainamide, propoxycaine, and naproxen were performed under acidic conditions with solvent A (H_2O + 0.1% HCOOH) and solvent B (95% ACN/5% H_2O + 0.1% HCOOH). Gradient for naproxen: 99% A from 0 min until 1 min; 99−0% A from 1.0 until 5.5 min and 0% A until 6.0 min. Gradient for procaine and procainamide and compounds: 99% A from 0 min until 1.0 min, 99−0% A from 1.0 until 3.5 min, and 0% A until 3.7 min. All LC separations were performed at a flow rate of 0.7 mL/min on an Agilent Zorbax Eclipse Plus 50 × 2.1 mm, 1.8 μm equipped with a guard column; temperature 60 °C (for **1**, **13**, **14**, **27a**, and **27b**) and 30 °C (for naproxen, procaine, procainamide, and propoxycaine). The MRM method was used for compound detection in the positive and negative modes. The Q1/Q3 transition masses used for compound identification are given in Table S3.

■ ASSOCIATED CONTENT

Supporting Information

The Supporting Information is available free of charge at https://pubs.acs.org/doi/10.1021/acsinfecdis.2c00523.

General chemical information; synthesis procedure of compounds **1**−**27**; fluorescently labeled bacteria and plots describing MIC curves; bacterial strains used in this study; MRM transitions for compounds **3**, **9**, and **10** for uptake experiments; quantifiers used for plasma stability and binding studies; and pictures of NMR spectra of intermediates and final compounds **4**−**7** for vancomycin conjugates, **9**−**12** for sorangicin conjugates, and **13**−**14** for the theranostic and imaging probes (PDF)

■ AUTHOR INFORMATION

Corresponding Author

Mark Brönstrup − *Department of Chemical Biology, Helmholtz Centre for Infection Research, 38124 Braunschweig, Germany; Institute for Organic Chemistry (IOC), Leibniz Universität Hannover, 30167 Hannover, Germany; German Center for Infection Research (DZIF), 38124 Braunschweig, Germany;* orcid.org/0000-0002-8971-7045; Email: Mark.Broenstrup@helmholtz-hzi.de

Authors

Carsten Peukert − *Department of Chemical Biology, Helmholtz Centre for Infection Research, 38124 Braunschweig, Germany*

Katharina Rox − *Department of Chemical Biology, Helmholtz Centre for Infection Research, 38124 Braunschweig, Germany; German Center for Infection Research (DZIF), 38124 Braunschweig, Germany*

Bianka Karge − *Department of Chemical Biology, Helmholtz Centre for Infection Research, 38124 Braunschweig, Germany*

Sven-Kevin Hotop − *Department of Chemical Biology, Helmholtz Centre for Infection Research, 38124 Braunschweig, Germany*

Complete contact information is available at: https://pubs.acs.org/10.1021/acsinfecdis.2c00523

Author Contributions

C.P. conceived the idea, conceptualized the study, synthetized and characterized all intermediates and conjugates, conducted cellular labeling and antimicrobial activity experiments, curated the biological and chemical data for publication, and wrote the manuscript. K.R. conducted the stability and plasma protein binding experiments and corrected and wrote the manuscript. S.-K.H. conducted and evaluated the subcellular quantification of compounds in bacteria by LC−MS/MS. B.K. conducted MIC and cytotoxicity assays. M.B. conceptualized the study, coordinated the research, and wrote the manuscript.

Funding

We acknowledge the funding by the Joint Program Initiative on Antimicrobial Resistance (JPI AMR, grant number: 01KI1825). C.P. thanks the "Fonds der chemischen Industrie" for a scholarship. K.R. and M.B. received support from the German Centre for Infection Research (DZIF, TTU 09.719 and TTU 09.722). We further acknowledge the support from the Helmholtz International Lab for anti-infectives.

Notes

The authors declare no competing financial interest.

■ ACKNOWLEDGMENTS

We thank Kirsten Harmrolfs and Christel Kakoschke for the measurement of NMR samples, Andrea Ahlers and Jennifer Wolf for technical assistance, and Ulrike Beutling for the mass spectrometric measurements. We are thankful to Marc Stadler and the Department of Microbial Drugs (MWIS) at the Helmholtz Centre for Infection Research for providing us sorangicin A.

■ ABBREVIATIONS

CuAAC, copper-catalyzed azide alkyne cycloaddition; DOTAM, tetrapodal 1,4,7,10-tetraazacyclododecane-1,4,7,10-tetraacetic amide; ENT, enterobactin; IDCAM, iron-depleted cation-adjusted medium; OMR, outer membrane receptor;

MIC, minimal inhibitory concentration; PCH, pyochelin; PG, phosphatidylglycerol; PPB, plasma protein binding; PVD, pyoverdine; RNAP, RNA-polymerase; TBDT, TonB-dependent transporters

REFERENCES

(1) Murray, C. J. L.; Ikuta, K. S.; Sharara, F.; Swetschinski, L.; Robles Aguilar, G.; Gray, A.; Naghavi, M. Global burden of bacterial antimicrobial resistance in 2019: a systematic analysis. *Lancet* **2022**, *399*, 629.

(2) Theuretzbacher, U.; Gottwalt, S.; Beyer, P.; Butler, M.; Czaplewski, L.; Lienhardt, C.; Moja, L.; Paul, M.; Paulin, S.; Rex, J. H.; Silver, L. L.; Spigelman, M.; Thwaites, G. E.; Paccaud, J. P.; Harbarth, S. Analysis of the clinical antibacterial and antituberculosis pipeline. *Lancet Infect. Dis.* **2019**, *19*, e40−e50.

(3) Tacconelli, E.; Carrara, E.; Savoldi, A.; Harbarth, S.; Mendelson, M.; Monnet, D. L.; Pulcini, C.; Kahlmeter, G.; Kluytmans, J.; Carmeli, Y.; Ouellette, M.; Outterson, K.; Patel, J.; Cavaleri, M.; Cox, E. M.; Houchens, C. R.; Grayson, M. L.; Hansen, P.; Singh, N.; Theuretzbacher, U.; Magrini, N.; Aboderin, A. O.; Al-Abri, S. S.; Awang Jalil, N.; Benzonana, N.; Bhattacharya, S.; Brink, A. J.; Burkert, F. R.; Cars, O.; Cornaglia, G.; Dyar, O. J.; Friedrich, A. W.; Gales, A. C.; Gandra, S.; Giske, C. G.; Goff, D. A.; Goossens, H.; Gottlieb, T.; Guzman Blanco, M.; Hryniewicz, W.; Kattula, D.; Jinks, T.; Kanj, S. S.; Kerr, L.; Kieny, M.-P.; Kim, Y. S.; Kozlov, R. S.; Labarca, J.; Laxminarayan, R.; Leder, K.; Leibovici, L.; Levy-Hara, G.; Littman, J.; Malhotra-Kumar, S.; Manchanda, V.; Moja, L.; Ndoye, B.; Pan, A.; Paterson, D. L.; Paul, M.; Qiu, H.; Ramon-Pardo, P.; Rodríguez-Baño, J.; Sanguinetti, M.; Sengupta, S.; Sharland, M.; Si-Mehand, M.; Silver, L. L.; Song, W.; Steinbakk, M.; Thomsen, J.; Thwaites, G. E.; van der Meer, J. W.; Van Kinh, N.; Vega, S.; Villegas, M. V.; Wechsler-Fördös, A.; Wertheim, H. F. L.; Wesangula, E.; Woodford, N.; Yilmaz, F. O.; Zorzet, A. Discovery, research, and development of new antibiotics: the WHO priority list of antibiotic-resistant bacteria and tuberculosis. *Lancet Infect. Dis.* **2018**, *18*, 318−327.

(4) Fleming, K. A.; Horton, S.; Wilson, M. L.; Atun, R.; DeStigter, K.; Flanigan, J.; Sayed, S.; Adam, P.; Aguilar, B.; Andronikou, S.; Boehme, C.; Cherniak, W.; Cheung, A. N. Y.; Dahn, B.; Donoso-Bach, L.; Douglas, T.; Garcia, P.; Hussain, S.; Iyer, H. S.; Kohli, M.; Labrique, A. B.; Looi, L.-M.; Meara, J. G.; Nkengasong, J.; Pai, M.; Pool, K.-L.; Ramaiya, K.; Schroeder, L.; Shah, D.; Sullivan, R.; Tan, B.-S.; Walia, K. The Lancet Commission on diagnostics: transforming access to diagnostics. *Lancet* **2021**, *398*, 1997.

(5) Klahn, P.; Brönstrup, M. Bifunctional antimicrobial conjugates and hybrid antimicrobials. *Nat. Prod. Rep.* **2017**, *34*, 832−885.

(6) Miethke, M.; Marahiel, M. A. Siderophore-based iron acquisition and pathogen control. *Microbiol. Mol. Biol. Rev.* **2007**, *71*, 413−451.

(7) Kramer, J.; Özkaya, Ö.; Kümmerli, R. Bacterial siderophores in community and host interactions. *Nat. Rev. Microbiol.* **2020**, *18*, 152−163.

(8) Ji, C.; Miller, M. J. Siderophore−fluoroquinolone conjugates containing potential reduction-triggered linkers for drug release: synthesis and antibacterial activity. *BioMetals* **2015**, *28*, 541−551.

(9) Zheng, T.; Nolan, E. M. Enterobactin-mediated delivery of beta-lactam antibiotics enhances antibacterial activity against pathogenic Escherichia coli. *J. Am. Chem. Soc.* **2014**, *136*, 9677−9691.

(10) Kim, A.; Kutschke, A.; Ehmann, D. E.; Patey, S. A.; Crandon, J. L.; Gorseth, E.; Miller, A. A.; McLaughlin, R. E.; Blinn, C. M.; Chen, A.; Nayar, A. S.; Dangel, B.; Tsai, A. S.; Rooney, M. T.; Murphy-Benenato, K. E.; Eakin, A. E.; Nicolau, D. P. Pharmacodynamic Profiling of a Siderophore-Conjugated Monocarbam in Pseudomonas aeruginosa: Assessing the Risk for Resistance and Attenuated Efficacy. *Antimicrob. Agents Chemother.* **2015**, *59*, 7743−7752.

(11) Ghosh, M.; Miller, P. A.; Möllmann, U.; Claypool, W. D.; Schroeder, V. A.; Wolter, W. R.; Suckow, M.; Yu, H.; Li, S.; Huang, W.; Zajicek, J.; Miller, M. J. Targeted Antibiotic Delivery: Selective Siderophore Conjugation with Daptomycin Confers Potent Activity against Multidrug Resistant Acinetobacter baumannii Both in Vitro and in Vivo. *J. Med. Chem.* **2017**, *60*, 4577−4583.

(12) Ghosh, M.; Lin, Y.-M.; Miller, P. A.; Möllmann, U.; Boggess, W. C.; Miller, M. J. Siderophore Conjugates of Daptomycin are Potent Inhibitors of Carbapenem Resistant Strains of Acinetobacter baumannii. *ACS Infect. Dis.* **2018**, *4*, 1529−1535.

(13) Ghosh, M.; Miller, P. A.; Miller, M. J. Antibiotic repurposing: bis-catechol- and mixed ligand (bis-catechol-mono-hydroxamate)-teicoplanin conjugates are active against multidrug resistant Acinetobacter baumannii. *J. Antibiot.* **2020**, *73*, 152−157.

(14) Pinkert, L.; Lai, Y. H.; Peukert, C.; Hotop, S. K.; Karge, B.; Schulze, L. M.; Grunenberg, J.; Brönstrup, M. Antibiotic Conjugates with an Artificial MECAM-Based Siderophore Are Potent Agents against Gram-Positive and Gram-Negative Bacterial Pathogens. *J. Med. Chem.* **2021**, *64*, 15440−15460.

(15) Ohi, N.; Aoki, B.; Kuroki, T.; Matsumoto, M.; Kojima, K.; Nehashi, T. Semisynthetic beta-lactam antibiotics. III. Effect on antibacterial activity and comt-susceptibility of chlorine-introduction into the catechol nucleus of 6-[(R)-2-[3-(3,4-dihydroxybenzoyl)-3-(3-hydroxypropyl)-1-ureido]-2- phenylacetamido]penicillanic acid. *J. Antibiot.* **1987**, *40*, 22−28.

(16) Chow, H. Y.; Po, K. H. L.; Jin, K.; Qiao, G.; Sun, Z.; Ma, W.; Ye, X.; Zhou, N.; Chen, S.; Li, X. Establishing the structure−activity relationship of daptomycin. *ACS Med. Chem. Lett.* **2020**, *11*, 1442−1449.

(17) Mühlberg, E.; Umstätter, F.; Kleist, C.; Domhan, C.; Mier, W.; Uhl, P. Renaissance of vancomycin: approaches for breaking antibiotic resistance in multidrug-resistant bacteria. *Can. J. Microbiol.* **2020**, *66*, 11−16.

(18) Jansen, R.; Schummer, D.; Irschik, H.; Höfle, G. Antibiotics from gliding bacteria, XLII. Chemical modification of sorangicin A and structure—Activity relationship I: Carboxyl and hydroxyl group derivatives. *Liebigs Ann. Chem.* **1990**, *1990*, 975−988.

(19) Ferreira, K.; Hu, H.-Y.; Fetz, V.; Prochnow, H.; Rais, B.; Müller, P. P.; Brönstrup, M. Multivalent siderophore−DOTAM conjugates as theranostics for imaging and treatment of bacterial infections. *Angew. Chem., Int. Ed.* **2017**, *56*, 8272−8276.

(20) Peukert, C.; Langer, L. N. B.; Wegener, S. M.; Tutov, A.; Bankstahl, J. P.; Karge, B.; Bengel, F. M.; Ross, T. L.; Brönstrup, M. Optimization of artificial siderophores as ^{68}Ga-complexed PET tracers for in vivo imaging of bacterial infections. *J. Med. Chem.* **2021**, *64*, 12359−12378.

(21) Peukert, C.; Popat Gholap, S.; Green, O.; Pinkert, L.; van den Heuvel, J.; van Ham, M.; Shabat, D.; Brönstrup, M. Enzyme-activated, chemiluminescent siderophore-dioxetane probes enable the selective and highly sensitive detection of bacterial pathogens. *Angew. Chem., Int. Ed.* **2022**, *61*, No. e202201423.

(22) Fritsch, S.; Gasser, V.; Peukert, C.; Pinkert, L.; Kuhn, L.; Perraud, Q.; Normant, V.; Brönstrup, M.; Schalk, I. Uptake mechanisms and regulatory responses to MECAM- and DOTAM-based artificial siderophores and their antibiotic conjugates in Pseudomonas aeruginosa. *ACS Infect. Dis.* **2022**, *8*, 1134.

(23) Pandey, A.; Savino, C.; Ahn, S. H.; Yang, Z.; Van Lanen, S. G.; Boros, E. Theranostic gallium siderophore ciprofloxacin conjugate with broad spectrum antibiotic potency. *J. Med. Chem.* **2019**, *62*, 9947−9960.

(24) Nosrati, R.; Abnous, K.; Alibolandi, M.; Mosafer, J.; Dehghani, S.; Taghdisi, S. M.; Ramezani, M. Targeted SPION siderophore conjugate loaded with doxorubicin as a theranostic agent for imaging and treatment of colon carcinoma. *Sci. Rep.* **2021**, *11*, 13065.

(25) Pfister, J.; Petrik, M.; Bendova, K.; Matuszczak, B.; Binder, U.; Misslinger, M.; Kühbacher, A.; Gsaller, F.; Haas, H.; Decristoforo, C. Antifungal siderophore conjugates for theranostic applications in invasive pulmonary aspergillosis using low-molecular TAFC scaffolds. *J. Fungi* **2021**, *7*, 558.

(26) Ho, S. W.; Jung, D.; Calhoun, J. R.; Lear, J. D.; Okon, M.; Scott, W. R.; Hancock, R. E.; Straus, S. K. Effect of divalent cations on the structure of the antibiotic daptomycin. *Eur. Biophys. J.* **2008**, *37*, 421−433.

https://doi.org/10.1021/acsinfecdis.2c00523
ACS Infect. Dis. 2023, 9, 330−341

(27) Heidary, M.; Khosravi, A. D.; Khoshnood, S.; Nasiri, M. J.; Soleimani, S.; Goudarzi, M. Daptomycin. *J. Antimicrob. Chemother.* **2017**, *73*, 1−11.
(28) Grein, F.; Müller, A.; Scherer, K. M.; Liu, X.; Ludwig, K. C.; Klöckner, A.; Strach, M.; Sahl, H.-G.; Kubitscheck, U.; Schneider, T. Ca^{2+}-daptomycin targets cell wall biosynthesis by forming a tripartite complex with undecaprenyl-coupled intermediates and membrane lipids. *Nat. Commun.* **2020**, *11*, 1455.
(29) Wu, Z.-C.; Cameron, M. D.; Boger, D. L. Vancomycin C-terminus guanidine modifications and further insights into an added mechanism of action imparted by a peripheral structural modification. *ACS Infect. Dis.* **2020**, *6*, 2169−2180.
(30) Okano, A.; Isley, N. A.; Boger, D. L. Peripheral modifications of [Ψ[CH_2NH]Tpg_4]vancomycin with added synergistic mechanisms of action provide durable and potent antibiotics. *Proc. Natl. Acad. Sci. U.S.A.* **2017**, *114*, E5052−E5061.
(31) Campbell, E. A.; Pavlova, O.; Zenkin, N.; Leon, F.; Irschik, H.; Jansen, R.; Severinov, K.; Darst, S. A. Structural, functional, and genetic analysis of sorangicin inhibition of bacterial RNA polymerase. *EMBO J.* **2005**, *24*, 674−682.
(32) Jansen, R.; Schummer, D.; Irschik, H.; Höfle, G. Antibiotics from gliding bacteria. Part 42. Chemical modification of sorangicin A and structure-activity relationship. Part 1. Carboxyl and hydroxyl group derivatives. *Liebigs Ann. Chem.* **1990**, *1990*, 975.
(33) Lilic, M.; Chen, J.; Boyaci, H.; Braffman, N.; Hubin, E. A.; Herrmann, J.; Müller, R.; Mooney, R.; Landick, R.; Darst, S. A.; Campbell, E. A. The antibiotic sorangicin A inhibits promoter DNA unwinding in a Mycobacterium tuberculosis rifampicin-resistant RNA polymerase. *Proc. Natl. Acad. Sci. U.S.A.* **2020**, *117*, 30423−30432.
(34) Ge, M.; Chen, Z.; Russell, H.; Onishi; Kohler, J.; Silver, L. L.; Kerns, R.; Fukuzawa, S.; Thompson, C.; Kahne, D. Vancomycin derivatives that inhibit peptidoglycan biosynthesis without binding $_d$-Ala-$_d$-Ala. *Science* **1999**, *284*, 507−511.
(35) Kerns, R.; Dong, S. D.; Fukuzawa, S.; Carbeck, J.; Kohler, J.; Silver, L.; Kahne, D. The role of hydrophobic substituents in the biological activityof glycopeptide antibiotics. *J. Am. Chem. Soc.* **2000**, *122*, 12608−12609.
(36) El-Mady, A.; Mortensen, J. E. The bactericidal activity of ampicillin, daptomycin, and vancomycin against ampicillin-resistant Enterococcus faecium. *Diagn. Microbiol. Infect. Dis.* **1991**, *14*, 141−145.
(37) Prochnow, H.; Fetz, V.; Hotop, S.-K.; García-Rivera, M. A.; Heumann, A.; Brönstrup, M. Subcellular quantification of uptake in Gram-negative bacteria. *Anal. Chem.* **2019**, *91*, 1863−1872.
(38) Pinkert, L.*Synthese von Siderophor-Antibiotika-Konjugaten als neuartige antibakterielle Wirkstoffe*. Hannover : Gottfried Wilhelm Leibniz Universität, Diss., **2020**, *VI*, 276.
(39) Ferreira, K.*Synthesis of siderophore-based conjugates to detect and treat bacterial infections*. Hannover : Gottfried Wilhelm Leibniz Universität, Diss., **2018**169.
(40) Krasavin, M.; Parchinsky, V.; Kantin, G.; Manicheva, O.; Dogonadze, M.; Vinogradova, T.; Karge, B.; Brönstrup, M. New nitrofurans amenable by isocyanide multicomponent chemistry are active against multidrug-resistant and poly-resistant Mycobacterium tuberculosis. *Bioorg. Med. Chem.* **2017**, *25*, 1867−1874.
(41) Wildermuth, R.; Speck, K.; Haut, F.-L.; Mayer, P.; Karge, B.; Brönstrup, M.; Magauer, T. A modular synthesis of tetracyclic meroterpenoid antibiotics. *Nat. Commun.* **2017**, *8*, 2083.

https://doi.org/10.1021/acsinfecdis.2c00523
ACS Infect. Dis. 2023, 9, 330−341